5G Coverage Optimization using Lower and Higher (mmWave) Frequency Bands

A. Alves
Instituto Superior Técnico,
University of Lisbon
Lisbon, Portugal
andre.q.alves@tecnico.ulisboa.pt

***Abstract*—This paper evaluates 5th Generation (5G) propagation models for Outdoor and Outdoor-to-Indoor (O2I) transitions, applying them to an open area and a Manhattan-like scenarios, at 3.5 and 28 GHz. In addition, Line-of-Sight (LOS) condition to a Base Station (BS) is assessed deterministically, and a novel 3D beamforming antenna model is proposed. The use of a massive Multiple Input Multiple Output (mMIMO) antenna and 3D beamforming allowed an average peak throughput of 3.23 Gbps at 28 GHz, although the Inter-Site Distance (ISD) must be shorter to ensure seamless coverage. In the presence of high-rise buildings, it is observed that radiation patterns with multiple vertical beams improved indoor coverage in, at least, 24.4%. Moreover, data from three measurement campaigns were employed to derive two calibrated models. The results show, in the worst case, a Mean Absolute Error (MAE) of 7.51 dB and a Root Mean Squared Error (RMSE) of 9.17 dB.**

***Index Terms*—5G, Propagation Models, Line-of-Sight, Pathloss, Beamforming, Calibration.**

I. Introduction

The past few years have witnessed a massive proliferation of mobile applications and services, which have caused a tremendous increase in mobile networks traffic. The 5th Generation (5G) is expected to benefit from the extension of used spectrum in order to improve network capacity and achieve high throughputs. The Third Generation Partnership Project (3GPP) defines two major frequency bands on which 5G will operate; Frequency Range (FR) 1, that accommodates the frequencies from 410 MHz to 7125 MHz, and FR2, from 24250 MHz to 52600 MHz, which include Millimeter Wave (mmWave) frequencies.

It is then crucial to be aware of propagation characteristics in these frequency bands in order to properly plan and optimize coverage. Therefore, many measurement campaigns have been performed by several institutions to accurately model propagation at 5G frequencies. Standard institutions usually develop omnidirectional pathloss models, *i.e.*, assuming the use of unity gain antennas [1]. However, concepts such as spatial multiplexing and 3D beamforming are key to enable 5G, hence these path loss models are not usable in directional antenna system analysis unless the antenna patterns are properly modeled [1]. The 3GPP antenna pattern model is the most common approach, with a horizontally-wide and vertically-narrow single beam [2], [3]. A new approach to beamforming antenna pattern modeling is proposed, enabling the simulation of antenna patterns with multiple beams and configurations.

The mobile industry has found benefitial to have separate pathloss models for Line-of-Sight (LOS) and Non Line-of-Sight (NLOS) conditions, due to the radio channel significant differences. Considering the newly available bands at higher frequencies, the LOS and NLOS propagation present even more distinct channels, especially at mmWaves [1]. Therefore, it is crucial to identify the LOS and NLOS areas to afterwards correctly apply the pathloss model. The most common approach is to use LOS probability models, *i.e.*, statistical models to predict the likelihood that a User Equipment (UE) is in a LOS condition with respect to the Base Station (BS). In [4], LOS/NLOS classification was done visually using Google Maps. In this paper, one benefits from increasingly available geodata to deterministically calculate whether or not a UE has LOS to the respective BS, thus ensuring a more reliable classification.

In this work, two propagation models, 3GPP and Millimetre-Wave Based Mobile Radio Access Network for Fifth Generation Integrated Communications (mmMAGIC), with different antenna patterns and at FR1 and FR2 frequencies, are applied to testing scenarios in order to assess coverage and throughput. Moreover, data from three sets of measurement campaigns are used to calibrate the models.

The paper is organized as follows: in Section II two antenna mask models are introduced; Section III presents the propagation models and the testing scenarios results; in Section IV the Drive Test (DT) data are analyzed and the models are calibrated. Finally, some conclusions are drawn in Section V.

II. Antenna Mask Models

The variation of a radio signal strength between the BS and a UE is described by propagation models. But as important as quantifying the losses in the propagation channel is to characterize both link ends, namely the BS antenna mask which results in the transmitting antenna gain.

This section starts by presenting the standard 3GPP antenna model, which is a simple model and allows a single beam, either in the horizontal and vertical planes.

Further on, due to the limitations of the 3GPP model, a new model was developed in the course of this work, enabling multiple beams in both horizontal and vertical planes.

A. 3GPP Antenna Model

This section describes the standard directional antenna pattern model, proposed by 3GPP to introduce 3D beamforming. The radiation pattern in the horizontal plane is given by:

$$G_H(\phi) = -\min\left\{12\left(\frac{\phi-\phi_{az}}{\phi_{3dB}}\right)^2, FBR\right\} \quad (1)$$

where ϕ ($\in [-180°, 180°]$) is the horizontal angle measured between the BS boresight and the line in the horizontal plane connecting the UE to the BS, ϕ_{az} denotes the fixed orientation angle of BS boresight relative to the x-axis, ϕ_{3dB} is the horizontal Half-Power Beamwidth (HPBW), and FBR is the front-to-back ratio.

Similarly, the vertical radiation pattern may be obtained as follows:

$$G_V(\theta) = -\min\left\{12\left(\frac{\theta-\theta_{tilt}}{\theta_{3dB}}\right)^2, SLL\right\} \quad (2)$$

where θ ($\in [-90°, 90°]$) is the vertical angle measured between the horizon and the line connecting the UE to the BS, θ_{tilt} denotes the antenna tilt and is measured between the horizon and the line passing through the peak of the beam, θ_{3dB} is the vertical HPBW, and SLL is the side-lobe level. Finally, the 3D antenna gain can be obtained as:

$$G_{BS}^{\text{dBi}}(\theta,\phi) = G_{\text{m}} - \min\{-[G_H(\phi)+G_V(\theta)], G_{\text{m}}\} \quad (3)$$

where G_{m} denotes the peak antenna gain.

B. Newly-developed Beamforming Antenna Model

As one of the main features of 5G, massive Multiple Input Multiple Output (mMIMO) antennas implement beamforming [5] to form extremely accurate user-level narrow beams. A mMIMO antenna can improve signal coverage and reduce interference between cells. This section presents a new approach in antenna modelling which is compatible with the 5G requirements and, although a simplified model, closer to the used 5G Active Antenna Systems (AASs).

In this model, both horizontal and vertical HPBW are the HPBW per beam. Therefore, if the horizontal and vertical HPBW read from an antenna datasheet are the total HPBW, then they must be divided by the number of horizontal and vertical beams, respectively, before being inputted to the model. The other model inputs are the number of horizontal (n_H) and vertical (n_V) beams, and the horizontal and vertical scanning range of beams, $[min_{range}, max_{range}]$, which are centered at the ϕ_{az} and at the θ_{tilt}, respectively.

The horizontal radiation pattern is obtained as follows:

$$G_H(\phi) = -\min\left\{12\left(\frac{\phi-k_H^{'}}{\phi_{3dB}}\right)^2, FBR\right\} \quad (4)$$

where $k_H^{'}$ is the angle at which an horizontal beam is centered, and is given by:

$$k_H^{'} = min_{range,H} + \phi_{A_{beam}}\left(\frac{1}{2}+i\right) \quad (5)$$

where $\phi_{A_{beam}}$ is given by:

$$\phi_{A_{beam}} = \frac{max_{range,H} - min_{range,H}}{n_H} \quad (6)$$

and i identifies the respective beam and is given by:

$$i = \min\{\lfloor \max(\phi - min_{range,H}, 0)/\phi_{A_{beam}} \rfloor, n_H - 1\} \quad (7)$$

Similarly, the vertical radiation pattern is obtained as follows:

$$G_V(\theta) = -\min\left\{12\left(\frac{\theta-k_V^{'}}{\theta_{3dB}}\right)^2, SLL\right\} \quad (8)$$

where $k_V^{'}$ is the angle at which an vertical beam is centered, and is given by:

$$k_V^{'} = min_{range,V} + \theta_{A_{beam}}\left(\frac{1}{2}+j\right) \quad (9)$$

where $\theta_{A_{beam}}$ is given by:

$$\theta_{A_{beam}} = \frac{max_{range,V} - min_{range,V}}{n_V} \quad (10)$$

and j identifies the respective beam and is given by:

$$j = \min\{\lfloor \max(\theta - min_{range,V}, 0)/\theta_{A_{beam}} \rfloor, n_V - 1\} \quad (11)$$

The 3D antenna gain G_{BS}^{dBi} is obtained from (3). An example of the application of this antenna model is shown in Fig. 1.

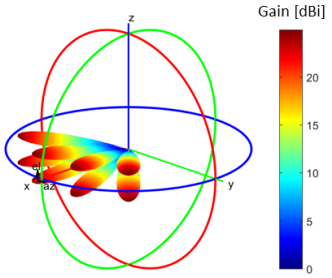

Fig. 1. Radiation Pattern (G_{m} = 25 dBi, 4 hor. beams, 2 vert. beams, $\phi_{3dB} = 11.25°$, $\theta_{3dB} = 12°$, hor. and vert. scanning range are [-60°,60°] and [-15°,15°], respectively.

III. Propagation Framework

This section starts off by describing the procedure to determine whether a UE is in LOS or NLOS to the respective BS. Afterwards, two propagation models, concerning outdoor propagation and Outdoor-to-Indoor (O2I) transitions, are introduced and employed in an open area and a Manhattan-like testing scenarios. The parameters of these two propagation models are given in Table I.

A. LOS/NLOS

Most 5G propagation models have different path loss equations for LOS and NLOS scenarios. In this paper, the author benefits from geodata (namely terrain and buildings [6]) to deterministically determine whether a UE is in LOS conditions to the BS or not, *i.e.*, whether the 1st Fresnel Ellipsoid radius is at least 60% clear or not [7]. The radius of the 1st Fresnel Ellipsoid in a point of the link between the BS and a UE which is distance z away from one of the terminals ($r_{1e,z}$), being obtained from:

$$r_{1e,z} = \sqrt{\lambda_c \frac{z(d_{2D} - z)}{d_{2D}}} \tag{12}$$

where λ_c is the wavelength and d_{2D} is the 2D distance between the BS and the UE. Afterwards, the difference between the height of the LOS beam and the geodata height at point z is computed:

$$\Delta h_z = h_{\text{geodata},z} - h_{\text{ray},z} \tag{13}$$

where $h_{\text{geodata},z}$ is the terrain plus buildings height at z and $h_{\text{ray},z} = mz + b$, with m and b being, respectively, the slope and intercept of the line equation of the LOS beam between BS and UE.

Finally, the condition which defines whether or not the 1st Fresnel zone obstruction at z is given by:

$$\text{Link} = \begin{cases} \text{NLOS} & \text{if } \Delta h_z > 0 \text{ or} \\ & (\Delta h_z < 0 \text{ and } |\Delta h_z| < 0.6 \cdot r_{1e,z}) \\ \text{LOS} & \text{otherwise} \end{cases} \tag{14}$$

The aforementioned procedure must be run iteratively over the link between the BS and a UE.

B. 3GPP TR 38.901

The 3GPP TR 38.901 pathloss models are valid from 0.5-100 GHz. The 3GPP Urban Micro (UMi) and Urban Macro (UMa) models for LOS conditions are breakpoint models, *i.e.*, have different equations depending on whether d_{2D} is smaller than the breakpoint distance d'_{BP} or not. The breakpoint distance can be defined as the distance from the BS where the 1st Fresnel ellipsoid touches the ground and the Pathloss Exponent (PLE) shifts from free space (PLE $= 2$) to the asymptotic two-ray ground bounce model (PLE $= 4$) [1]. The LOS breakpoint distance d'_{BP} in meters is given by:

$$\begin{aligned} d'_{\text{BP}} &= 4h'_{\text{BS}}h'_{\text{UE}}/\lambda_c \\ h'_{\text{BS}} &= h_{\text{BS}} + h_{\text{geodata,BS}} - h_{\text{geodata,UE}} \\ h'_{\text{UE}} &= h_{\text{UE}} \end{aligned} \tag{15}$$

In NLOS conditions, the 3GPP pathloss models follow the Alpha-Beta-Gamma (ABG) modeling, with an additional correction term for the UE height. The UMi and UMa model parameters are presented in Table I.

Moreover, the Shadow Fading (SF) for the 3GPP models follow a log-normal distribution (see standard deviation σ_{SF} in Table I).

The 3GPP TR 38.901 [3] also has a O2I penetration loss model, which is useful to describe the additional losses that an indoor UE may experience. Thereby, the pathloss experienced by an indoor user may be modeled as follows:

$$PL = PL_{\text{b}} + PL_{\text{tw}} + PL_{\text{in}} + N(0, \sigma_P^2) \tag{16}$$

where PL_{b} is the basic outdoor pathloss, where d_{3D} is replaced by $d_{3D\text{-out}}$ and $d_{3D\text{-in}}$ (outdoor and indoor 3D distance, respectively); PL_{tw} is the building penetration loss through the external wall; PL_{in} is the inside loss dependent on the depth into the building; and σ_P is the standard deviation for the penetration loss. The penetration loss is derived by:

$$PL_{\text{tw}} = PL_{\text{npi}} + 10\log_{10}\sum_{i=1}^{N}\left(p_i \times 10^{-\frac{L_{\text{material},i}}{10}}\right) \tag{17}$$

where PL_{npi} is an additional loss added to the external wall loss to account for non-perpendicular incidence, which is 5 dB in the 3GPP model, p_i is the proportion of the i-th material, $\sum p_i = 1$, $L_{\text{material},i} = \text{a}_{\text{material},i} + \text{b}_{\text{material},i} \cdot f_c$ is the penetration loss of material i, where f_c is the frequency in GHz, and N is the number of materials. Penetration loss of several materials may be found in [3].

Two O2I penetration loss models are provided in [3]: a low-loss and a high-loss model, depending on the building materials. In this work, an intermediate model is used, where both models contribute with 50% to the total loss.

C. mmMAGIC

The mmMAGIC models omnidirectional pathloss from 6-100 GHz [8]. The UMi pathloss also follows the ABG modeling and the distribution of the SF is log-normal. The model parameters are provided in Table I.

The O2I building penetration loss model is basically the same as the corresponding model agreed in 3GPP [3]. There are, however, a couple of additional terms introduced:

- a log-normal frequency dependent spread $\sigma_{\text{P}}^{\text{dB}} = 4 + k_\sigma f_c$ where k_σ is building dependent.
- a term to account for elevation angle loss $L_{el} = 20\,|\theta/90°|$.

D. Testing Scenarios

The propagation models are now applied in several scenarios at 3.5 and 28 GHz, using different antenna patterns, and coverage and peak throughput [9] are analyzed. It is assumed 2 MIMO layers and no carrier aggregation. At 3.5 GHz, it is used a 100 MHz bandwidth and numerology 2, while at 28 GHz, 400 MHz bandwidth and numerology 3 are assumed. The used BS antennas are: Kathrein 742212, which is a sectorial antenna ($G_{\text{m}} = 18$ dBi, $\phi_{3dB} = 63°$, $\theta_{3dB} = 6.5°$), and the AAU5613, which is a mMIMO antenna with a 8×12 phased array, allowing multiple-beam radiation patterns ($G_{\text{m}} = 25$ dBi). Antenna tilts were not object of optimization, and are such that the vertical gain is 6 dB below the maximum in the horizon direction.

TABLE I
UMA AND UMI PATHLOSS MODELS

Model		PL [dB], f_c [GHz], d [m]	σ_{SF} [dB]	Applicability range and default values
3GPP UMa [3]	LOS	$PL_{\text{UMa-LOS}} = \begin{cases} PL_1 & \text{if } 10 \text{ m} \leq d_{2D} \leq d_{BP}^{'} \\ PL_2 & \text{if } d_{BP}^{'} < d_{2D} \leq 5 \text{ km} \end{cases}$ $PL_1 = 28 + 22\log_{10}(d_{3D}) + 20\log_{10}(f_c)$ $PL_2 = 28 + 40\log_{10}(d_{3D}) + 20\log_{10}(f_c)$ $- 9\log_{10}((d_{\text{BP}}^{'})^2 + h_{eff}^2)$	4	$0.5 < f_c < 100$ GHz $10 < d_{2D} < 5000$ m $1.5 \leq h_{\text{UE}} \leq 22.5$ m $h_{\text{BS}} = 25$ m
	NLOS	$PL_{\text{UMa-NLOS}} = \max\left(PL_{\text{UMa-LOS}}, PL_{\text{UMa-NLOS}}^{'}\right)$ $PL_{\text{UMa-NLOS}}^{'} = 13.54 + 39.08\log_{10}(d_{3D}) + 20\log_{10}(f_c)$ $- 0.6\log_{10}(h_{\text{UE}} - 1.5)$	6	
3GPP UMi [3]	LOS	$PL_{\text{UMi-LOS}} = \begin{cases} PL_1 & \text{if } 10 \text{ m} \leq d_{2D} \leq d_{BP}^{'} \\ PL_2 & \text{if } d_{BP}^{'} < d_{2D} \leq 5 \text{ km} \end{cases}$ $PL_1 = 32.4 + 21\log_{10}(d_{3D}) + 20\log_{10}(f_c)$ $PL_2 = 32.4 + 40\log_{10}(d_{3D}) + 20\log_{10}(f_c)$ $- 9.5\log_{10}((d_{\text{BP}}^{'})^2 + h_{eff}^2)$	4	$0.5 < f_c < 100$ GHz $10 < d_{2D} < 5000$ m $1.5 \leq h_{\text{UE}} \leq 22.5$ m $h_{\text{BS}} = 10$ m
	NLOS	$PL_{\text{UMi-NLOS}} = \max\left(PL_{\text{UMi-LOS}}, PL_{\text{UMi-NLOS}}^{'}\right)$ $PL_{\text{UMi-NLOS}}^{'} = 22.4 + 35.3\log_{10}(d_{3D}) + 21.3\log_{10}(f_c)$ $- 0.3\log_{10}(h_{\text{UE}} - 1.5)$	7.82	
mmMAGIC UMi [8]	LOS	$PL_{\text{UMi-LOS}} = 32.9 + 19.2\log_{10}(d_{3D}) + 20.8\log_{10}(f_c)$	2	$6 < f_c < 100$ GHz $1.5 \leq h_{\text{UE}} \leq 3$ m $1.5 \leq h_{\text{BS}} \leq 10$ m
	NLOS	$PL_{\text{UMi-NLOS}} = 31 + 45\log_{10}(d_{3D}) + 20\log_{10}(f_c)$	7.82	

1) Open Area: The open area testing scenario consists of 19 3-sectorized sites (BSs) displayed in a hexagonal grid and flat terrain without obstacles. The UE height is always assumed to be 1.5 m and outdoor, and LOS and NLOS propagation are analysed separately. Two different configurations are simulated: a UMa scenario and a UMi scenario.

The UMa scenario is characterized by a 500 m Inter-Site Distance (ISD), BS height is 25 m, and their transmitting power is 40 W. At 3.5 GHz, coverage is very close to 100% both in LOS and NLOS conditions, whereas at 28 GHz coverage barely surpasses 20% in NLOS for the best covering antenna pattern (AAU5613, 8 hor. beams and 1 vert. beam, 110° hor. HPBW, 12° hor. HPBW). On the other hand, at 28 GHz, it is possible to attain very high throughputs, as the AAU5613 reaches an average throughput of 3.23 Gbps in LOS and 1 Gbps in NLOS and nearly 100 Mbps in the cell edge, outperforming the Kathrein 742212 (3.1 Gbps in LOS and 0.22 Gbps in NLOS).

The UMi scenario is characterized by a 200 m ISD, BS height is 10 m, and their transmitting power is 20 W. The reduced ISD allows an improved coverage at 28 GHz (52% for the best antenna pattern) although insufficient, reinforcing the idea that for mmWaves, small cells and LOS may be necessary. Again, the AAU5613 antenna outperforms the Kathrein 742212, and higher throughputs are also achieved, with 3.5 Gbps in LOS and 1.8 Gbps in NLOS, and 835 Mbps in the cell edge for the best pattern. Moreover, when comparing the 3GPP and the mmMAGIC models, the latter's 50% percentile NLOS pathloss is 26 dB lower, which is a significant difference.

2) Manhattan-like: The Manhattan-like scenario has been widely used for multiple radio technologies. A slightly modified Manhattan-like scenario is used (Fig. 2). Sidewalks (in dark brown) around the buildings (light brown) were added, separating them from the road. Thus, this Manhattan-like scenario consists of a 5x5 building grid, where the building width is 40 m and the street is 20 m wide (16 m for road width and 2 m for each sidewalk width). Buildings are 25 m height, and are divided in 8 floors considering that each floor is 3 m height, and the sidewalks are 0.2 m height. The BSs height is 10 m, and are located on lampposts in the middle of the sidewalks (*i.e.* 1 m away from the building wall and 1 m away from the road edge), which are assumed to be regularly displayed along the sidewalks. For the sake of simplicity, in Fig. 2 only the lampposts which give support the the BS are represented (black dots). The terrain is assumed to be flat.

Link budget calculations were performed to determine the maximum ISD to ensure coverage in worst case, which is an indoor UE at 28 GHz. This results in a maximum distance of around 96 m. Thus, and following the display in [10], there are 15 3-sectorized BS with an average ISD of 92.5 m, as shown in Fig. 2.

Due to link budget planning, near 100% outdoor and indoor coverage is attained at both 3.5 and 28 GHz. While, at 3.5 GHz, the average outdoor and indoor peak throughput is 761 and 349 Mbps, respectively, at 28 GHz the values are significantly higher. At 28 GHz, the average outdoor and indoor peak throughput is 2.98 and 1.05 Gbps, respectively, and the outdoor and indoor cell edge throughput peak at 2.2

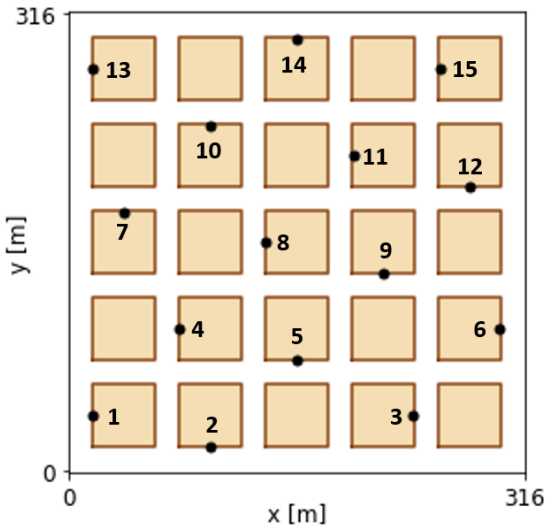

Fig. 2. Manhattan-like scenario.

Gbps and 67 Mbps, respectively. The antenna downtilt also plays an important role in coverage planning. In this work, the tilt was set so that the antenna radiates 6 dB below the maximum vertical gain in the horizon in order to improve outdoor coverage. Therefore, the antenna pattern that shows better results is the AAU5613 antenna with 8 hor. beams and 1 vert. beam, 110° hor. HPBW, and 12° hor. HPBW. However, as far as indoor UEs are concerned, the radiation pattern in Fig. 1 shows a performance almost as good as the aforementioned radiation pattern. Hence, had tilt optimization been done concerning also indoor UEs, the best antenna pattern for indoor coverage would be the pattern in Fig. 1.

E. Lisbon

The purpose of this scenario is to demonstrate how areas with distinct morphology may require different antenna parameters for an improved coverage. Amongst the simulated scenarios in Lisbon are an area in Saldanha with a large building density, with an average height of 20.1 m, and a hotel in Picoas which is 92 m tall, and it is considered that a dedicated cell from a BS is used. The BS is on a nearby building, and is at a 26 m height. All simulations are performed at 3.5 GHz.

Saldanha Area

Firstly, the Saldanha area is studied. The first test performed is the comparison between Pattern 1 and Pattern 9. In the previous testing scenarios the antenna parameters were kept constant, namely the scanning ranges of beams and the antenna tilt, which was set so that the vertical beam radiates 6 dB below the maximum gain in the horizon direction; however, in this scenario, tilt values from 0° to 12° are tested, as well as two different vertical scanning ranges of beams.

The results for the Saldanha area are shown in Figures 3 and 4. For Pattern 1, since it only has one vertical beam, changing the vertical scanning range does not affect the

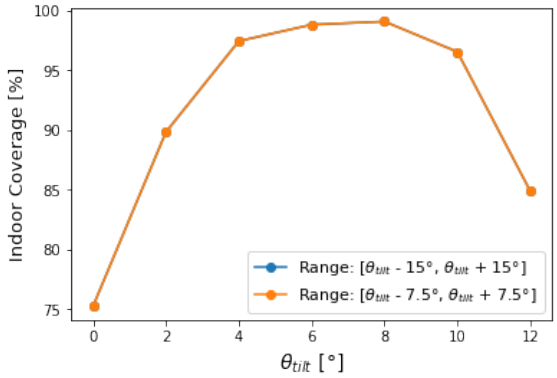

Fig. 3. Saldanha Indoor Coverage with Pattern 1.

radiation pattern. With smaller tilt values, the indoor coverage is smaller, but as the tilt increases the radiation pattern is more pointed to the buildings hence almost full indoor coverage is attained. When the tilt is very high, the radiation pattern points to the ground, deteriorating indoor coverage.

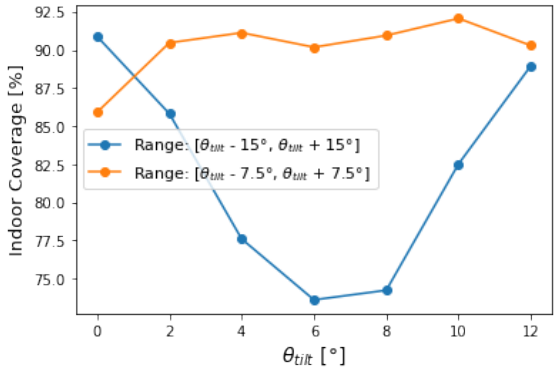

Fig. 4. Saldanha Indoor Coverage with Pattern 9.

As for Pattern 9, the two scanning ranges provide distinct results. The radiation pattern with the range [$\theta_{tilt} - 15°$, $\theta_{tilt} + 15°$] and 0○ tilt behaves as Pattern 1 (but with 4 horizontal beams only) because the lower vertical beam points to the buildings whereas the upper beam radiates energy to the ”air”. As the tilt increases, the lower beam points more to the ground while the upper beam does not point yet in the direction where most buildings would be covered, hence indoor coverage deteriorates. When the maximum of the upper beam radiates at a higher elevation angle, indoor coverage improves again. With a smaller vertical scanning range of beams, [$\theta_{tilt} - 7.5°$, $\theta_{tilt} + 7.5°$], indoor coverage is almost constant around 90%. The wider the vertical scanning range of beams, the more dispersed the radiated energy. Thus with the smaller range, the radiated energy is more focused around the tilt angle, and the radiation pattern minimum is higher than with the previous range. There are still the variations that there were in the [$\theta_{tilt} - 15°$, $\theta_{tilt} + 15°$] range, but they are much smaller. Therefore, one concludes that having a wider range of beams may not always be beneficial due to the high

energy dispersion. In addition, these simulations showed the difference in the tilt concept which was described above.

From the results above, one must find odd that the radiation pattern that provides the highest percentages of indoor coverage is Pattern 1, which has only one vertical beam, when compared to radiation patterns with multiple beams. The explanation is actually a simple one: the eight horizontal beams of Pattern 1 provide better coverage across the cell's service area, which is mainly comprised by indoor areas (buildings). With the use of mmWaves, the 5G network will be immensely densified with micro and small cells, and some cells will not have to cover larger areas, especially in highly populated and densely built areas with high-rise buildings and skyscrapers, where the radiation patterns with multiple vertical beams will truly improve indoor coverage when compared to a radiation pattern such as Pattern 1.

It may also be concluded that changing the radiation pattern *per se* may not produce the results one could expect. The analysis must be broader than that: the geometry of the problem, *i.e.*, the area to be covered and the characteristics of that area, the BS(s) location and height, the scanning range of beams, and the antenna tilt.

Picoas Area

In the Picoas area, it is only simulated the indoor coverage of one particular building. It is a well-known hotel in Lisbon and one of the tallest buildings in the city, with a 92 m height, and the aim is to demonstrate that radiation patterns with multiple beams truly outperform single-beam patterns in such scenarios. Assuming an uniform distribution of UEs, the tilt is set so that it points approximately to the middle of the building. The horizontal scanning of beams is $[\phi_{az} - 25°, \phi_{az} + 25°]$, and the vertical scanning of beams is $[\theta_{tilt} - 15°, \theta_{tilt} + 15°]$.

The results are presented in Figure 5. As shown in the figure,

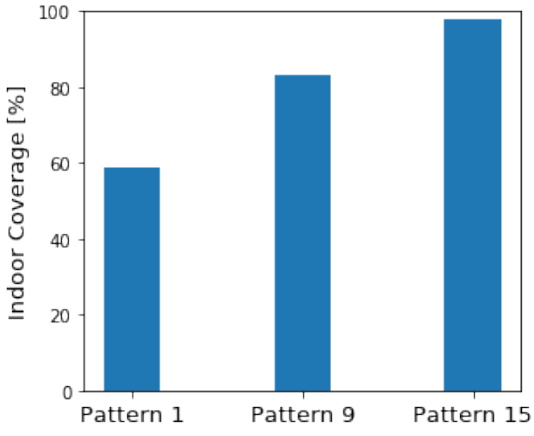

Fig. 5. Picoas Indoor Coverage, with several radiation patterns.

from Pattern 1 to Pattern 9 there is a major improvement in the building indoor coverage, from 58.7% to 83.1%. With such a narrow horizontal scanning range of beams, Pattern 1 is able to provide almost maximum gain across the building, however only in one direction. However, the building height is almost twice its width, hence covering in the vertical plane is more important than in the horizontal direction to the overall indoor coverage. A simulation with Pattern 15 (2 horizontal and 4 vertical beams), which is a radiation pattern with 2 horizontal beams and 4 vertical beams, improved the indoor coverage even more, attaining 97.8%.

A top view fooprint of the Reference Signal Received Power (RSRP) per floor is showed in Figure 6, and it is visible how the signal varies from floor to floor[1].

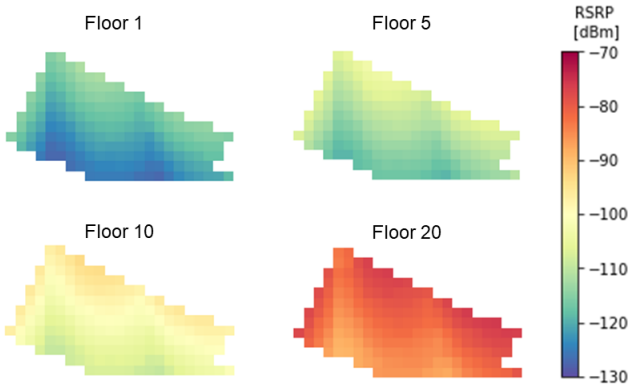

Fig. 6. RSRP per floor of the high-rise building in Picoas for Pattern 9.

IV. Calibration

There is usually some disagreement between the values which result from the use of an empirical model and the actual measured data for a specific area. Propagation models are usually based on extensive measurement campaigns, which are strongly dependent on the specific geographical area (*e.g.*, heavy clutter or other topological peculiarities [11]), frequency band, or weather conditions.

In order to have a better coverage and network planning, the propagation model parameters must be optimized for each geographical location or for several similar ones. DT data are used to compare with the predicted results, and based on that comparison, calibrate the propagation models using the linear regression algorithm.

A. Drive Tests

Three DT datasets were used: one in Ciudad Real, Spain, and the others in Italy (Milan and Ivrea). The Ciudad Real DT was performed at 3.7 GHz and there are a total of 3 sites and 4 sectors at a 20 m height. The Milan and Ivrea DTs were performed at 26 GHz, the data concerns to one sector for each DT, and the BS are 30 m and 15 m height, respectively. All samples are outdoor and are taken at a 1.5 m height.

The first step towards models calibration was to obtain geodata for the aforementioned locations, and thereupon input it to the LOS algorithm (Section III-A) to separate the data by

[1]Due to technical issues which could not be fixed in due time, the building is not fully represented in the figure.

LOS and NLOS. Fig. 7 exemplifies the procedure described, and visually confirms the outcome of the LOS algorithm.

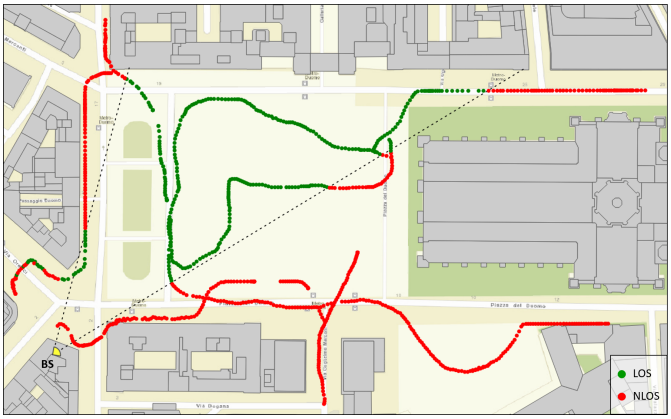

Fig. 7. Milan DT classified in LOS and NLOS.

Afterwards, the pathloss is derived from the measured UE received power, the downlink reference signal power, and the 3D antenna gain, which is determined using the model in Section II-B knowing the antennas used for the DTs.

B. Slow Fading Filtering

Propagation models describe the average pathloss experienced in a mobile radio environment. However, field measurements are instantaneous, hence they include slow fading (shadowing) and fast fading (multipath). Measured data S may then be modeled as:

$$S(t) = M(t) + R(t) \tag{18}$$

where M is the mean pathloss and R denotes a fading term. Therefore, before making any comparisons between the DT measurements and propagation models, a sliding-window algorithm is employed to filter R out. Fast fading is not considered since it is out of the scope of this work.

The filtering process can be carried out by averaging the samples over a spatial and temporal range of samples where the mean signal (pathloss) is considered to be constant. Let S_i be the ith sample. Hence, the ith estimated mean $\hat{M}_i$ is

$$\hat{M}_i = \frac{1}{|X|} \sum_{k=\min(X)}^{\max(X)} S_k \tag{19}$$

where $X = \{n : d(S_i, S_n) \leq L \wedge t(S_i, S_n) \leq \Delta t\}$. The parameters $d(S_i, S_n)$ and $t(S_i, S_n)$ are the distance and time interval between samples S_i and S_n, respectively; $\Delta t = L/v$ and L define the window size and are the maximum time interval and distance, respectively, where the signal is considered to be sensibly constant, v is the average DT speed. According to [12], L must be between 20 and 40λ.

C. Linear Regression

In this work, only the 3GPP UMa model was calibrated. All BSs heights are much higher than the default values for the 3GPP and mmMAGIC UMi, except in the Ivrea DT. However, this DT only has 14 LOS samples, which is not enough for calibration, thus only NLOS calibration would be possible.

All DT samples were found to fall short of the breakpoint distance. Thus, since the 3GPP UMa model (LOS PL_1 and NLOS) is ABG-type, linear regression was the method chosen to perform the model calibration. Two calibrated models were derived:

- A **Full-Spectrum model**, *i.e.*, for FR1 and FR2, where all DTs are included in the dataset. Both LOS and NLOS may be modeled as:

$$PL = 10\alpha \log_{10}(d_{3D}) + \beta + 10\gamma \log_{10}(f_c) \tag{20}$$

- A **26 GHz model**, where only the Italy DTs are used for calibration. Modeling is the same as in (20), but since f_c is constant it may be rewritten as in (21), simplifying the regression.

$$PL = 10\alpha \log_{10}(d_{3D}) + \nu \tag{21}$$

where $\nu = \beta + 10\gamma \log_{10}(28)$.

The Python library `scikit-learn` with the Sum of Squared Errors (SSE) as cost function was used to perform the linear regressions. The results are presented in Table II and compared to the original pathloss model.

TABLE II
MODEL CALIBRATION RESULTS

	α	β	γ	MAE	RMSE	R^2
3GPP UMa Model						
LOS	2.2	28	2	21.05	23.42	-
NLOS	3.908	13.54	2	14.48	16.66	-
Full-Spectrum Model						
LOS	4.53	20.87	0.40	5.45	7.26	0.50
NLOS	3.8	24.67	2.46	7.51	9.17	0.58
26 GHz Model						
LOS	4.71	-5.45	2	5.0	7.08	0.56
NLOS	3.78	31.78	2	7.16	8.71	0.53

The results for LOS conditions are far from what was expected, with a high PLE while it should be closer to free space propagation. This may be explained by the few LOS samples in the Ciudad Real DT, and whose received power appear to be lower than usual, perhaps because of destructive interference. This leads, on one hand to, a very small γ, and on the other hand, to a larger α. In the 26 GHz model, the offset value is a negative value, nonetheless in ABG modeling, β has no physical meaning, being only an optimization parameter.

Generally, Mean Absolute Error (MAE) and Root Mean Squared Error (RMSE) are improved after the model calibration, and the coefficient of determination R^2 ranges from 0.50 to 0.58. There are some associated errors to the calibration procedure which may prevent the results to be better: there was some uncertainty relative to the BSs downtilt; the used antenna

model is only a simplified model thus some inaccuracies are expected; the LOS algorithm may also have experienced some errors due to the buildings data spatial display being slightly imprecise, and the buildings height in Ciudad Real and Ivrea had a lower resolution.

If one had access to DTs in the area of Lisbon where geodata are available, then calibrated models could be derived and used in Section III-E to perform the simulations instead of the propagation models from Section III, thus providing more trustworthy results.

V. Conclusions

This paper presents a UMa and two UMi 5G propagation models, as well as a O2I penetration loss model. Furthermore, a novel antenna mask model, prepared to deal with 3D beamforming, is introduced, and a deterministic approach to determine LOS or NLOS is used. The results for the testing scenarios show that on one hand, FR1 frequencies provide a compromise between coverage and throughput, but on the other hand, higher frequencies (FR2) are the key to unlock the full potential of 5G, making use of larger bandwidth to attain throughput up to 3.23 Gbps. In addition, the use of 3D beamforming helps to overcome the higher losses at 5G frequencies by enabling high-gain directive beams.

Additionally, three measurement campaigns and respective geodata were analyzed in order to calibrate the UMa model. The data fading component was removed using a sliding-window filtering algorithm, and Linear Regression was then applied to determine the model parameters which minimize the SSE. Two models were obtained: a full-spectrum model, with a MAE of 7.51 dB and a RMSE of 9.17 dB (worst case); and a 28 GHz model , with a MAE of 7.16 dB and a RMSE of 8.71 dB (worst case). Thus, when performing simulations at 26 GHz, the latter model should be used since it is based only on measurements for that frequency, and it provides the smaller error.

Acknowledgment

An acknowledgment is due to CELFINET and Instituto de Telecomunicações (IT) for the support to this work.

References

[1] T. S. Rappaport, Y. Xing, G. R. MacCartney, A. F. Molisch, E. Mellios and J. Zhang, "Overview of Millimeter Wave Communications for Fifth-Generation (5G) Wireless Networks—With a Focus on Propagation Models," in *IEEE Transactions on Antennas and Propagation*, vol. 65, no. 12, pp. 6213-6230, Dec. 2017.

[2] N. Seifi, J. Zhang, R. W. Heath, T. Svensson and M. Coldrey, "Coordinated 3D Beamforming for Interference Management in Cellular Networks," in *IEEE Transactions on Wireless Communications*, vol. 13, no. 10, pp. 5396-5410, Oct. 2014.

[3] 3GPP TR 38.901, Study on channel model for frequencies from 0.5 to 100 GHz, 3GPP, October 2019, 16.0.0.

[4] S. Sun, T. A. Thomas, T. S. Rappaport, H. Nguyen, I. Z. Kovacs and I. Rodriguez, "Path Loss, Shadow Fading, and Line-of-Sight Probability Models for 5G Urban Macro-Cellular Scenarios," *2015 IEEE Globecom Workshops (GC Wkshps)*, San Diego, CA, 2015, pp. 1-7.

[5] P. Vieira, M. P. Queluz, A. Rodrigues, "MIMO antenna array impact on channel capacity for a realistic macro-cellular urban environment", 68th *IEEE Vehicular Technology Conference (VTC – Fall 2008)*, Calgary, Canada, September 2008.

[6] P. Vieira, M. P. Queluz, A. Rodrigues, "A dynamic propagation prediction platform over irregular terrain and buildings for wireless communications", 66th *IEEE Vehicular Technology Conference (VTC – Fall 2007)*, Baltimore, USA, October 2007.

[7] Carlos Salema, *Microwave Radio Links*, 1st edition, John Wiley and Sons Inc, 2002.

[8] mmMAGIC D2.2, "Measurement Results and Final mmMAGIC Channel Models", v2.0, ICT-671650, mmMAGIC Project, 2017.

[9] 3GPP TS 38.306, User Equipment (UE) radio access capabilities, 3GPP, October 2018.

[10] 3GPP TR 25.942, RF System Scenarios, 3GPP, June 2006.

[11] P. Vieira, M. P. Queluz, A. Rodrigues, "Clustering of scatterers over an irregular clutter environment: an extension of COST 273 MIMO channel model", 66th *IEEE Vehicular Technology Conference (VTC – Fall 2007)*, Baltimore, USA, October 2007.

[12] W. C. Y. Lee, "Estimate of local average power of a mobile radio signal," in *IEEE Transactions on Vehicular Technology*, vol. 34, no. 1, pp. 22-27, Feb. 1985.